Journal of Biomechanics 88 (2019) 155–163

Contents lists available at ScienceDirect

Journal of Biomechanics

journal homepage: www.elsevier.com/locate/jbiomech
www.JBiomech.com

A biomechanically derived minimum work model of the fish gill lamellar system exhibits its exquisite morphological arrangement and perfusate regulation for oxygen uptake from water

Akira Kamiya [a], Kimiko Yamamoto [b,*]

[a] Research Laboratory for Interdisciplinary Sciences, Tokyo, Japan
[b] Department of Biomedical Engineering, Graduate School of Medicine, University of Tokyo, Tokyo, Japan

ARTICLE INFO

Article history:
Accepted 26 March 2019

Keywords:
Aquatic respiration
Fish gill lamellar system
Oxygen uptake
Oxygen consumption
Rainbow trout

ABSTRACT

To evaluate the efficiency of oxygen (O_2) uptake from water through the fish gill lamellar system, a cost function (*CF*) representing mechanical power expenditure for water ventilation and blood circulation through the gill was formulated, by applying steady-state fluid mechanics to a homogeneous lamellar-channel model. This approach allowed us to express *CF* as the function of inter-lamellar water channel width (w) and to derive an analytical solution of the width (w_{min}) at the minimum *CF*. Morphometric and physiological data for rainbow trout in the literature were referred to calculate $CF(w)$ curves and their w_{min} values at five intensity stages of swimming exercise. Obtained w_{min} values were evenly distributed around the standard measure of the width (w_s = 24 μm) in this fish. Individual levels of $CF(w_{min})$ were also fairly close to the corresponding $CF(w_s)$ values within a 10% deviation, suggesting the reliability of approximating $[CF(w_{min}) = CF(w_s)]$. The cost-performance of O_2 uptake through the gill (η_g) was then assessed from reported data of total O_2 uptake/$CF(w_s)$ at each intensity stage. The η_g levels at any swimming stage exceeded 95% of the theoretical maximum value, implying that O_2 uptake is nearly optimally performed in the lamellar-channel system at all swimming speeds. Further analyses of O_2 transport in this fresh water fish revealed that the water ventilation by the buccal/opercular pumping evokes a critical limit of swimming velocity, due to confined O_2 supply to the peripheral skeletal muscles, which is avoided in ram ventilators such as tuna.

1. Introduction

Among various physiological functions performed in fish gills (Evans et al., 2005), oxygen (O_2) uptake from water must be one of the most fundamental activities continuously supporting the aquatic life. However, the physical conditions under which gills extract O_2 from water are much more strenuous than those under which lungs in terrestrial animals breath air, because air contains approximately 20% O_2, whereas water has no more than 0.6% O_2 (Eckert et al., 1988; Hill et al., 2016; Schmidt-Nielsen, 1990). Furthermore, the viscosity of water, which is proportional to mechanical work required for fluid ventilation, is approximately 150 times greater than that of air. Despite such physical constraints, sufficient amount of O_2 is supplied to fish blood via gills because O_2 tension in the dorsal aorta is maintained at a comparable level to that in large systemic arteries in mammals (around 100 mm Hg) (Davis and Cameron, 1971; Malte and Weber, 1985).

The high affinity of fish blood to O_2 (Root et al., 1939; Schmidt-Nielsen, 1990) is considered to be one of the major factors that facilitate O_2 delivery from water to blood. The morphological arrangement of the gill lamellar microstructure is also closely related to this function (Hughes, 1966, 1972; Hughes and Morgan, 1973). The gill is composed of several gill arches, from each of which many gill filaments protrude (Fig. 1). On both surfaces of every filament, a number of gill lamellae of nearly the same size and shape are aligned in uniform rows. This compact gill lamellar system is the essential site for gas exchange between water and blood by diffusion. Fig. 1 also shows that the direction of blood flow through the vascular bed inside the lamellae is opposite to that of the water flow through the inter-lamellar channels. This counter-current arrangement provides an effective mechanism for O_2 transport from water to blood (Eckert et al., 1988; Hill et al., 2016; Malte and Weber, 1985).

* Corresponding author at: Hongo 7-3-1, Bunkyo-ku, Tokyo 113-0033, Japan.
E-mail addresses: a-kamiya@umin.ac.jp (A. Kamiya), k-yamamoto@umin.ac.jp (K. Yamamoto).

https://doi.org/10.1016/j.jbiomech.2019.03.033
0021-9290/

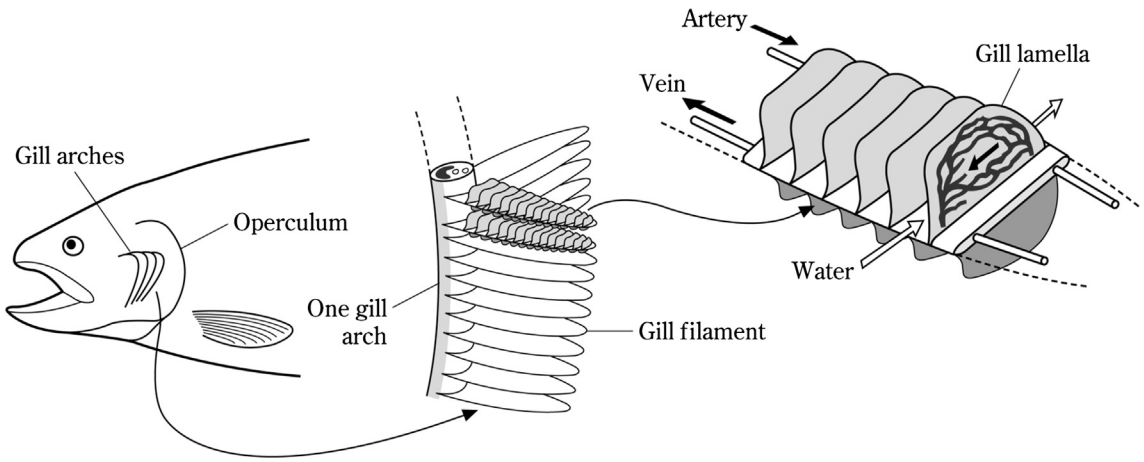

Fig. 1. Cascade illustrations of the fish gill anatomy (modified from Schmidt-Nielsen, 1990). The gill consists of several gill arches, from each of which protrude many gill filaments. On both sides of every filament surface, a number of nearly uniform gill lamellae are aligned with an even interval to form a ladder-like row. Note that the direction of blood flow through the vascular bed inside the lamellae is opposite to that of water flow through the inter-lamellar channels. This countercurrent system plays an important role in O_2 transport from water to blood by diffusion.

An important factor that may significantly affect the biomechanical efficiency of gill respiration is the density of gill lamellae on the filaments, or more directly, the width of the inter-lamellar water channels. Lamella density is typically proportional to gill surface area and more active fish species usually have more surface areas per body mass than less active species. (Wegner, 2011). However, if the density is too high and the width of the inter-lamellar space is too narrow, immense mechanical power may be required for water ventilation through the gill. By contrast, if the density is too low and the blood flow rate through each single lamella becomes too large, the mechanical power cost for blood circulation through the intra-lamellar vascular beds may increase proportionally as a whole. Furthermore, water channels that are too wide may present a risk that a substantial amount of water may flow through them in vain without contributing any O_2 transfer to blood, because the zone relevant to O_2 diffusion toward the lamellar surface (diffusion boundary layer) is physically limited to a certain adjacent zone to the surface (Caro and Nerem, 1973). Therefore, it is important to analyze the effects of water channel width on the mechanical power cost of gill respiration and to utilize the results for estimating the cost performance of O_2 uptake by "the ratio of the acquired amount of O_2/required mechanical power cost". This ratio is also closely related to the amount of O_2 supplied to exercising skeletal muscles for swimming.

In this study, steady-state fluid dynamics were applied to the terminal flows in the gills. The biomechanical power expenditure for water ventilation and blood circulation through the gill lamellar system was then evaluated as the cost function (*CF*) for respiration. The consequence of *CF* analyses using morphological and physiological data in rainbow trout in many reports (e.g., Hughes, 1966; Kiceniuk and Jones, 1977) allowed us to determine the efficiency of the teleost gill lamellar system in O_2 uptake from water and examine potential limiting factor of O_2 supply to contracting muscles during swimming.

2. Methods

2.1. Theoretical analyses

(a) Minimum work model of the gill lamellar system

Based on a simple anatomical structure of the gill (Fig. 1), we introduced a common geometrical model of a single lamellar-channel unit (Fig. 2). Every lamella stands upright on the surface

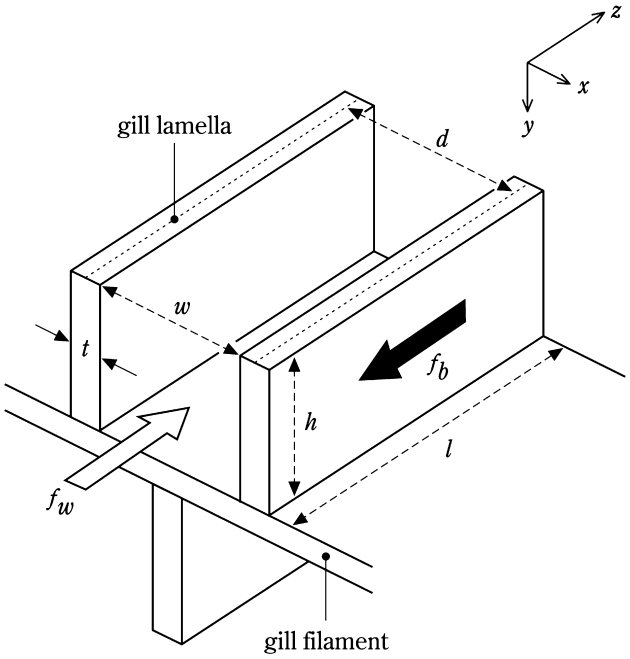

Fig. 2. A schematic diagram of the morphological model of the gill lamella-channel unit employed in the theoretical analyses. The parameters of the plate-like lamella (l, h, t and d) designate its length, height, thickness and distance to the next and the parameter (w) indicates the width of the channel space between the two neighboring lamellae. The symbols (f_b) and (f_w) represent the volumetric blood and water flow rates through a single unit, respectively.

and perpendicular to the long axis of each gill filament at an equal distance (d) from the next. The lamellae have a uniform rectangular plate shape with the same height (h), length (l), and thickness (t). Thus, every channel between two neighboring lamellae forms a straight and oblong channel for water flow with a uniform width (w), which is expressed as [$w = d - t$]. The channels are not covered with solid plates at the top but are in contact with the top surface flux through similar channels placed opposite of each other. Therefore, the channel model is essentially identical to the conventional pore model proposed by Hughes (1966).

The characteristics of the water and blood pressure-flow relationships were analyzed by applying steady state fluid mechanics.

(See the theoretical verification in Appendix A.) The results were utilized to formulate the total biomechanical power expenditure for the entire gill as the cost function for respiration (CF).

When the water channel width (w) was selected as the main variable of CF, the final outcome of the theoretical treatments (Appendix A; from Eqs. (A-1)–(A-7)) afforded us the following expression:

$$CF(w) = \Delta P_w F_w + \Delta P_b F_b = R_w F_w^2 + R_b F_b^2 = 3\frac{l}{h}\frac{\mu_w}{L_g}\left(\frac{1}{h^2}+\frac{4}{w^2}\right)F_w^2 + \frac{r_b w}{L_g}F_b^2 \quad (1)$$

where (ΔP_w and ΔP_b) and (R_w and R_b) are the hydraulic pressure drop and the resistance against total volumetric water and blood flow rates (F_w and F_b) over the gills, respectively, while (μ_w) indicates the viscosity of water. The term (L_g) represents the total sum of the inter-lamellar channel width ($L_g = nw$), where n denotes the total number of channels.

By assuming that all parameters except (w) in Eq. (1) are constant, the channel width ($w_{\min}$) that minimizes $CF(w)$ can be determined from $[\partial CF(w)/\partial w = 0]$, which renders an explicit analytical solution of $w_{\min}$ as follows:

$$w = \left[24\frac{\mu_w}{r_b}\frac{l}{h}\left(\frac{F_w}{F_b}\right)^2\right]^{1/3} = w_{\min} \quad (2)$$

(Appendix A; Eq. (A-8))

Moreover, the resistance (r_w) to water flow through a single channel ($f_w = F_w/n$) can be derived from Eq. (1) and approximated as follows:

$$r_w = \frac{\Delta P_w}{f_w} = 3\frac{l}{h}\frac{\mu_w}{w}\left(\frac{1}{h^2}+\frac{4}{w^2}\right) \approx 12\frac{l}{h}\frac{\mu_w}{w^3} \quad (3)$$

because $1/h^2 << 1/w^2$.

(b) Cost performance and relative efficiency of O_2 uptake through the gills

It is possible to evaluate the cost performance of O_2 uptake from water via the gill (η_g) by using total amount of O_2 uptake per unit time ($\dot{Q}$) through the gills and the cost function $CF(w)$ in Eq. (1) as follows:

$$\eta_g = \frac{\dot{Q}}{CF(w)} \quad (4)$$

It is also well documented that the above $\dot{Q}$ is predominantly regulated by total volumetric water ventilation (F_w) (Evans et al., 2005) and can be expressed with the constant parameters k_0 and $\alpha(\ll 1)$ as follows:

$$\dot{Q} = k_0 F_w^{1-\alpha} \quad (5)$$

Further analyses on the cost performance in Appendix B (from Eqs. (A-10)–(A-16)) have revealed that the relative efficiency (η_g^*), defined as η_g normalized with its maximum value ($\eta_{g,\max}$), can be expressed as a unique function of total volumetric water/blood flow ratio [$\xi = F_w/F_b$] with R_w and R_b in Eq. (1) and α in Eq. (5) as follows:

$$\eta_g^*(\xi) = \frac{\eta_g}{\eta_{g,\max}} = \left(\frac{\xi^{1-\alpha}}{R_w\xi^2 + R_b}\right)\Big/\left(\frac{\varphi^{1-\alpha}}{R_w\varphi^2 + R_b}\right) \quad \text{where } \varphi = \left[\frac{(1-\alpha)}{(1+\alpha)}\frac{R_b}{R_w}\right]^{1/2}. \quad (6)$$

It is apparent that when $\xi = \varphi$, $\mu_g^*(\xi) = 1$.

(c) Regulation of peripheral O_2 supply

When a fish is trying to swim faster, it is a crucial physiological problem whether sufficient O_2 can be supplied to peripheral exercising muscles or not. The amount of O_2 supply to peripherals ($\Delta\dot{Q}$) is equal to the residual of total O_2 uptake ($\dot{Q}$) minus the amount of O_2 consumed by the gill itself. This self-consumption rate of O_2 can be written as [$\kappa CF(w)$], using a coefficient (κ) converting the mechanical power expenditure to O_2 consumption rate. Thus, $\Delta\dot{Q}$ is expressed from Eqs. (1) and (5) as follows:

$$\Delta\dot{Q} = \dot{Q} - \kappa CF(w) = k_0 F_w^{1-\alpha} - \kappa(R_w F_w^2 + R_b F_b^2) \quad (7)$$

Regarding the two independent variables (F_w and F_b) in Eq. (7), if their responses *in vivo* are almost linearly correlated (as verified in Eq. (S-3) in Supplement 1) and their relationship can be expressed using two constant parameters (β and γ) as

$$F_b = \beta F_w + \gamma \quad (8)$$

$\Delta\dot{Q}$ is given as a quadratic function of F_w,

$$\Delta\dot{Q} = k_0 F_w^{1-\alpha} - \kappa\left[R_w F_w^2 + R_b(\beta F_w + \gamma)^2\right]$$

which allows to determine its maximizing condition of $\Delta\dot{Q}$ by differentiating the above with respect to F_w and setting the outcome to zero;

$$\frac{d}{dF_w}(\Delta\dot{Q}) = k_0(1-\alpha)F_w^{-\alpha} - 2\kappa[(R_w + R_b\beta^2)F_w + R_b\beta\gamma] = 0 \quad (9)$$

Eq. (9) was used to quantify the value of κ in Eq. (13) based on the $\Delta\dot{Q}$ curve in Fig. 5 in Results.

(d) Diffusion boundary layer

According to Caro and Nerem (1973) and Ando et al. (1993), the magnitude of the O_2 diffusion boundary layer (δ_d) in the water channel is expressed as follows:

$$\delta_d \approx 1.5\left(\frac{9\cdot D\cdot\mu_w\cdot z}{\bar{\tau}_s}\right)^{1/3} \text{ where } \bar{\tau}_s = 6\frac{\mu_w f_w}{w^2 h}, \quad (10)$$

in which (D) indicates O_2 diffusivity in water, and (z) designates the distance from the inlet of the water channel while ($\bar{\tau}_s$) represents the mean wall shear stress on the lamellar surface induced by a single channel water flow (f_w) (Appendix A; Eq. (A-3)).

2.2. Numerical assessments of relevant parameters for model analyses

To obtain numerical solutions for Eqs. (1)–(10), we used a number of physical, morphological, and physiological data, as being listed in Tables 1 and 2 with source references.

The top two columns in Table 1 list the physical parameters (D and μ_w at 10 °C), which are followed by morphometric data of the gill lamellar system (l, h, w, etc.); the latter were selected from data reported for rainbow trout of body weight around 1 kg in the cited references. The estimates of the total number of lamellae, the aggregate sum of their surface area in the whole gills (N and A_g), and the hydraulic resistances against volumetric blood and water flow rates over a single unit or the entire gills (r_b, r_w and R_b, R_w) are also summarized in Table 1 with the references. (See Supplement 1 for details of their numerical assessments.)

Table 2 lists the mean values of *in vivo* measures about relevant physiological variables, such as ($\dot{Q}$), (F_b) and (F_w) in rainbow trout of body weights of 0.9–1.5 kg (Kiceniuk and Jones, 1977). These measurements were performed after sustaining the subject fish at a given swimming velocity (U) for 1 hr. (See Supplement 1 for

Table 1
Physical, morphological and fluid-mechanical data in rainbow trout of body weight around 1 kg used for various numerical calculations and assessments (1 μm = 10^{-4} cm).

Parameters	Numerical values	References
Viscosity of water (μ_w) at 10 °C	1.3×10^{-2} dyn · s/cm^2	
O_2 diffusivity (D) in water at 10 °C	1.5×10^{-5} cm^2/s	
Length of a single gill lamella (l)	650 μm	(1)
Height of a single gill lamellae (h)	200 μm	(1)
Width of an inter-lamellar water lane (w)	24 μm	(2),(3)
The observed range of water lane width ($\tilde{w}$)	(20 ~ 25) μm	(3)
The observed range of lamellar thickness ($\tilde{t}$)	(20 ~ 35) μm	(3)
Total surface area of gill lamellae (A_g)	2.0×10^3 cm^2	(2),(3)
Total number of gill lamellae (N)	7.7×10^5	(2),(3)
Accumulated length of gill lamellae (L_g)	185 cm	(2),(3)
Blood flow resistance through the entire gill (R_b)	4.13×10^4 dyn · s/cm^5	(4)
Water flow resistance through the entire gill (R_w)	4.77×10^1 dyn · s/cm^5	(3),(4)
Resistance against a single lamellar blood flow (r_b)	3.19×10^{10} dyn · s/cm^5	(2),(4)
Resistance against a single channel water flow (r_w)	3.67×10^7 dyn · s/cm^5	
The resistance ratios; $\frac{k_2}{k_1} = \frac{r_b}{r_w} = \frac{R_b}{R_w}$	8.66×10^2	(2),(4)

The references: (1) Evans et al., 2005; (2) Hughes, 1972; (3) Hughes & Morgan, 1973; (4) Kiceniuk & Jones, 1977.

details of the measuring processes.) The obtained physiological data were classified into five groups according to the intensity of the applied exercise (Stages I-V), which was assorted by the range of the velocity index (λ), given as the percent ratio of U to the critical (maximum) velocity (U_{crit}) as,

$$\lambda = U/U_{crit} \times 100(\%) \tag{11}$$

Table 2 also lists their several derivatives, as explained in Results.

Five individual sets of $\dot{Q}$, F_b and F_w data (Table 2) were used to determine their mutual empirical relationships (Eqs. (5) and (8)) statistically. The values of involved parameters (k_0, α, β, γ) are listed in Table 2 (See Supplement 1, Eqs. (S-2) and (S-3)).

3. Results

The water channel width ($w_{\min}$) which minimized $CF(w)$ was calculated from Eq. (2) by substituting the data of (μ_w, r_b, l, h) in Table 1 and the flow ratio (F_w/F_b) in Table 2 for each of the five Stages. The results in Table 2 showed that the $w_{\min}$ values at Stage I (λ = 0%), II (λ = 41%–63%), III (λ = 70%–78%), IV (λ = 81%–91%), and V (λ = 92%–100%) were 16.3, 23.6, 24.1, 29.5, and 32.3 μm, respectively. These values were almost evenly distributed around the standard channel width ($w_s \approx 24$ μm) in Table 1.

The cost function curve $CF(w)$ was also calculated from Eq. (1) for each Stage by employing the value of the total sum of the water channel width (L_g) estimated from the total number of inter-lamellar channels ($N = 7.7 \times 10^5$) in 1 kg rainbow trout (Supplement 1) and the standard channel width ($w_s \approx 24$ μm), as $L_g = Nw_s \approx 1850$ cm. The calculated $CF(w)$ curves in Fig. 3 showed that as the stage number increased, the curves shifted to higher levels, together with the $CF(w_{\min})$ values. The descending slopes of the curves in the range ($w \leqslant w_{\min}$) were very steep, mainly due to abrupt decreases in water flow resistances, whereas the ascending slopes in the range ($w \geqslant w_{\min}$) were rather moderate reflecting gradual increases in blood flow resistances associated with increased vascular wall shear stress.

Based upon such characteristics of $CF(w)$ curves, we attempted to evaluate the difference between $CF(w_s)$ and $CF(w_{\min})$ with the extra cost rate (ε) defined as,

$$\varepsilon = [CF(w_s)/CF(w_{\min}) - 1] \times 100\,(\%) \tag{12}$$

The results in Table 2 revealed that at all Stages (I–V), the ε values never exceeded the level of 10%, although the values at rest (Stage I) was slightly modified by taking into account of vascular recruitment observed at the onset of the shift from the resting to swimming states (Olson, 2002). (Supplement 1, Eq. (S-2′)). Thus, the reliability of approximating [$CF(w_{\min}) \approx CF(w_s)$] was confirmed in all Stages within a 10% deviation.

Fig. 4 illustrates the results of the relative efficiency curve $\eta_g^*(\xi)$ calculated from Eq. (6) and plotted against the flow ratio ($\xi = F_w/F_b$). It was obvious either from Fig. 4 or in Table 2 that

Table 2
Physiological data for total blood and water flow rates through the gill based on *in vivo* measures under sustained exercise at various swimming velocities in rainbow trout of body weights normalized as 1.0 kg (modified from data by Kiceniuk and Jones, 1977).

Stage	λ (%)	n_e	$\dot{Q}$ (mlO$_2$/s)	F_b(ml/s)	F_w(ml/s)	F_w/F_b (ξ)	$w_{\min}$ (μm)	ε (%)	η_g^*	κCF (mlO$_2$/s)	$\Delta\dot{Q}$ (mlO$_2$/s)
I	0	9	0.93×10^{-2}	0.293	3.43	11.7	18.7	5.84	0.71	0.28×10^{-2}	0.65×10^{-2}
II	41–63	3	2.53×10^{-2}	0.473	9.66	20.4	23.7	0.01	0.95	0.75×10^{-2}	1.78×10^{-2}
III	70–78	5	3.17×10^{-2}	0.580	12.20	21.0	24.1	0.00	0.96	1.03×10^{-2}	2.14×10^{-2}
IV	81–91	3	5.20×10^{-2}	0.715	20.35	28.5	29.5	4.63	1.00	2.26×10^{-2}	2.95×10^{-2}
V	92–100	4	7.23×10^{-2}	0.877	28.62	32.6	32.3	9.99	0.99	4.03×10^{-2}	3.20×10^{-2}

(1) λ: Velocity index defined by Eq. (11).
(2) n_e: Number of experiments for physiological data measurements.
(3) $\dot{Q}$: Total O_2 consumption rate per 1 kg body weight.
(4) F_b: Total blood flow rate (cardiac output) per 1 kg body weight.
(5) F_w: Total water flow rate (gill ventilation) per 1 kg body weight estimated from $\dot{Q}$data (Eq. (5)).
(6) $w_{\min}$: The water lane width minimizing the cost function (CF) (Eq. (2)).
(7) ε: The excessive rate of CFat the standard lane width ($w_s = 24$ μm) (Eq. (12)).
(8) η_g^*: The relative efficiency of O_2 uptake through the gill sieve (Eq. (6)).
(9) κCF: O_2 consumption rate for gill respiration, where (κ) ($= 5.57 \times 10^{-7}$ mlO$_2$/dyn/cm) is the converting coefficient of biomechanical power cost to O_2 consumption rate (Eq. (13)).
(10) $\Delta\dot{Q}$: The amount of O_2 supplied to the peripherals defined by [$\Delta\dot{Q} = \dot{Q} - \kappa CF$] (Eq. (7)).
(11) Parameters in empirical relationships.
(i) $\dot{Q} = k_0 F_w^{1-\alpha}$; $k_0 = 2.83 \times 10^{-3}$, $\alpha = 3.3 \times 10^{-2}$ (Eqs. (5) and (S-2)).
(ii) $F_b = \beta F_w + \gamma$; $\beta = 2.25 \times 10^{-2}$, $\gamma = 25.3 \times 10^{-2}$ (Eqs. (8) and (S-3)).
(12) The size of O_2 diffusion boundary layer ($\sigma_d \geqslant 24.8$ μm) (Eq. (15)).

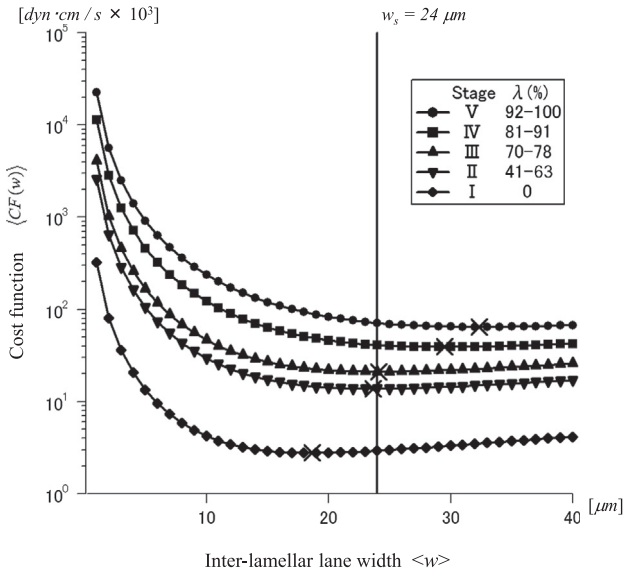

Fig. 3. The cost function curves $CF(w)$ calculated as the function of the inter-lamellar channel width (w) from Eq. (1) using the data of rainbow trout of body weight about 1 kg in Table 2 (Kiceniuk and Jones, 1977). The curves are plotted for five different Stages (Stage I, II, II, IV and V) clustered by the fish swimming velocity index ($\lambda = U/U_{crit} \times 100\%$) (Eq. (11)), where U and U_{crit} indicate the recoded and maximum (critical) velocities, respectively. The individual ranges of λ at Stage I ~ V are (0%, 41–63%, 70–78%, 81–91%, 92–100%) as listed in Table 2. The letters (x) designate the points at the minimum levels of the individual curves, $\langle CF(w_{min})\rangle$. In all curves, the descending slopes in the range ($w \leqslant w_{min}$) were very steep, mainly due to abrupt decreases in water flow resistances, whereas the ascending slopes in the range ($w \geqslant w_{min}$) were rather moderate due to gradual increases in blood flow resistances associated with increased vascular wall shear stress. The vertical straight line represents the most often observed, standard channel width ($w_s = 24\mu m$).

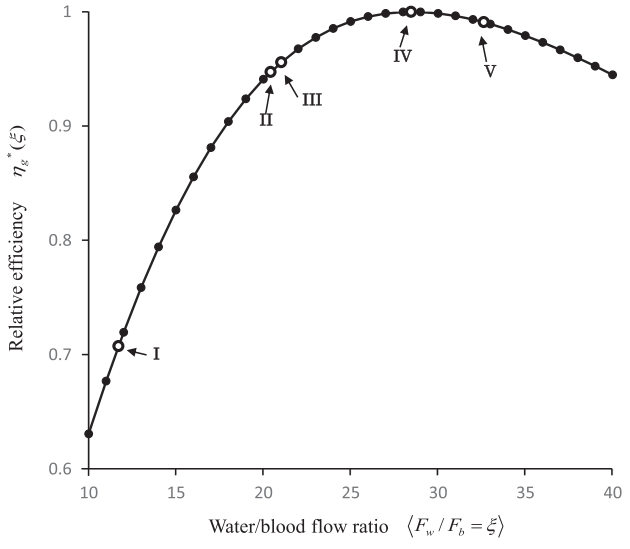

Fig. 4. The relative efficiency curve of O_2 uptake from water through the gill, $\eta_g^*(\xi)$, in Eq. (6) plotted against the water/blood flow ratio ($F_w/F_b = \xi$) with solid points (●). The blank circles (○) indicate the relative efficiency levels at Stages I, II, III, IV and V in Table 2, respectively. As the Stage rises from I to IV with the increase in ξ from 11.7 to 21.0, the relative efficiency levels gradually elevates but passes over the summit of the unity between Stage IV and V at $\xi = \xi_{max} = 28.6$ and then decreases toward Stage V at $\xi = 32.6$ on the descending slope.

the efficiency levels were higher than 0.95 at Stages II–V ($40\% \leqslant \lambda \leqslant 100\%$). These facts suggested that the responses of F_b and F_w were so finely coordinated during swimming Stages that very high efficiency levels were maintained by adjusting their ratio (ξ) quite close to the optimum value [$\xi = \phi = 28.5$] from Eq. (6), affording the highest efficiency [$\eta_g^*(\xi) = 1.0$].

Fig. 5 depicts three curves relevant to O_2 transport at rest and during swimming states: (i) total O_2 uptake ($\dot{Q}$), (ii) O_2 consumption by the gill (κCF), and (iii) O_2 supply to peripherals ($\Delta\dot{Q} = \dot{Q} - \kappa CF$). They are plotted as unique functions of total water ventilation (F_w) by utilizing the empirical $F_w - F_b$ relationship in Eq. (8) (or Eq. (S-3) in Supplement 1).

It is shown in Fig. 5 that as F_w increases, both $\dot{Q}$ and κCF elevate, but their rising patterns are different. The $\dot{Q}$ curve shows an almost linear slope, whereas the κCF curve reveals a quadratic profile as suspected from Eq. (1). Consequently, the residual $\Delta\dot{Q}$ curve exhibits a concave pattern with a peak. This summit of the $\Delta\dot{Q}$ curve reflects the situation at Stage V, because the critical (maximum) swimming velocity (U_{crit}) must be elicited by the maximum O_2 supply to the peripheral exercising muscles. Accordingly, the value of κ is estimated from Eq. (9) by substituting the value of ($F_w = 28.6\,\text{ml/s} = F_{crit}$) at Stage V and the values of (k_0, α, β, γ) in Table 2 as,

$$\kappa = \frac{k_0 w(1-\alpha)(F_{crit})^{-\alpha}}{2\left[(R_w + R_b\beta^2)F_{crit} + R_b\beta\gamma\right]} = 5.57 \times 10^{-7}(\text{mlO}_2/\text{dyn/cm}) \quad (13)$$

In the estimation of the size of the O_2 diffusion boundary layer (σ_d) against the maximum water flow rate ($F_w = F_{crit} = 28.6$ ml/s) at Stage V, the mean wall shear stress at the lamellar wall surface ($\bar{\tau}_s$) is estimated from Eq. (10) with the parameters in Table 1 as,

$$\bar{\tau}_s = 6\frac{F_{crit}\mu_w}{Nw^2h} = 25.2\,\text{dyn/cm}^2 \quad (14)$$

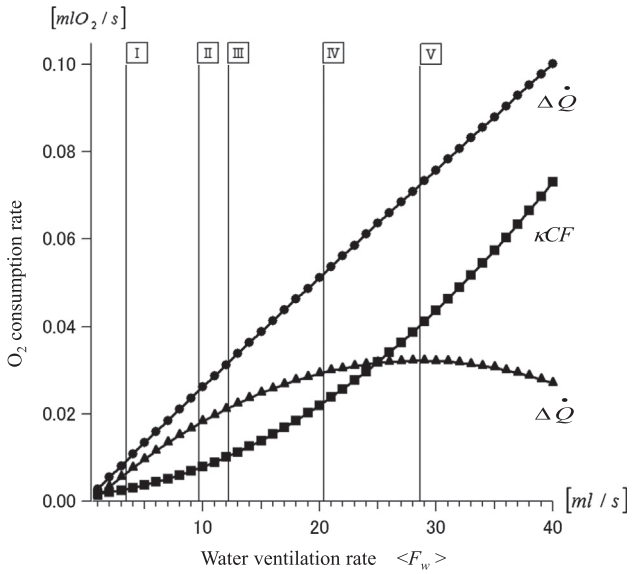

Fig. 5. Three curves of O_2 consumption rates obtained in about 1 kg rainbow trout are plotted against the total water ventilation rate (F_w); (i) total O_2 uptake from water ($\dot{Q}$) by Eq. (5); (ii) O_2 consumption rate due to the gill respiration (κCF) by Eqs. (1) and (13); and (iii) O_2 supply to peripherals ($\Delta\dot{Q}$) by Eq. (7), all based on the empirical $F_w - F_b$ relationship in Eq. (8) and in Table 2 (or Eq. (S-3) in Supplement 1). With the increase in F_w, the $\dot{Q}$ curve elevates nearly linearly whereas the increasing slope of the κCF curve is steep and quadratic, and therefore, the curve of $\Delta\dot{Q}(= \dot{Q} - \kappa CF)$ exhibits a concave profile. The vertical lines designate five Stages (I, II, III, IV and V) clustered by the swimming velocity index (λ) as shown in Fig. 3 and Table 2. Note that the summit of the $\Delta\dot{Q}$ curve at $F_w = F_{crit} = 28.6$ ml/s crosses with the vertical line of the Stage V, according to the estimate of $\kappa = 5.57 \times 10^{-7}$ mlO$_2$/(dyn · s) by Eq. (13).

Accordingly, the σ_d value at the exit of the water channel ($z = l = 650$ μm) is calculated from Eq. (10) with physical parameters (D and μ_w) in Table 1 as follows;

$$\delta_d = 1.5\left(\frac{9 \cdot D \cdot \mu_w \cdot z}{\bar{\tau}_s}\right)^{1/3} = 24.8 \times 10^{-4}\,\text{cm} \approx 25\,\mu\text{m} \qquad (15)$$

The above σ_d value, which is approximately twice as much as the length from the center of the water flux to the lamellar surface ($\sigma_d \geqslant w_s/2 = 12$ μm), is large enough to eliminate the risk that the central water fluxes may flow through the channel in vain without contributing any O_2 transfer to blood. It is also apparent that the same conclusion is applicable to lower Stages of swimming activity because the σ_d levels increase at lower $\bar{\tau}_s$ or F_w values.

4. Discussion

To confirm the validity of the findings shown in Results, the reliability of several assumptions introduced in the theoretical analyses must first be examined.

As the microstructural model of the gills, we adopted a homogeneous inter-lamellar channel unit (Fig. 2). However, its actual architecture has been reported to be fairly heterogeneous, varying in shapes, sizes and densities of lamellae along the longitudinal axis of the filament, besides the species-specific variations in their profiles (Hughes, 1984; Hughes and Morgan, 1973). Nevertheless, a homogeneous and compact morphological model was an essential requisite for theoretical and physiological comprehension of the fundamental system functions (Malte, 1989).

A steady-state pressure-flow relationship for water flux through the inter-lamellar channel was assumed to formulate the biomechanical power cost (CF) in Eq. (1). However, many experimental studies (Hughes, 1960; Hughes and Shelton, 1958; Malte, 1989; Strother, 2013a, b) have demonstrated pulsatile pressure waves in distal and proximal portions of the gills corresponding to the buccal/opercular pumping cycle in such fresh water fish as rainbow trout. Nevertheless, with respect to the water fluxes in the inter-lamellar spaces, the application of the steady-state flow model has been verified, because of very low Reynolds number at that sites (Malte, 1989; Wegner, 2011). (See the verification in Appendix A.) Similarly, blood flow inside the lamella is assumed to be steady as in mammalian capillary flow (Shibata et al., 2005).

Another major assumption used in the CF calculation was that the water flux shunting outside the inter-lamellar channels could be excluded from the water ventilation through the entire gill. However, Hughes (1966) and Strother (2013a,b) claimed that the total resistance to water flow actually measured over the gill in tench was much greater than the theoretical estimate by the pore model they adopted and that the excessive resistance should be ascribed to the shunting flow outside the gill lamellar system. To confirm such massive shunting flow bypassing the gill channels, we considered it necessary to reexamine the assessing process of water flow resistance over the entire gills, by supplementing new theoretical findings obtained in the present channel model.

The results of comparisons between the values of total water flow resistance by the pore model, by the channel model, and by the *in vivo* measurements in two specimens (140 g tench and 1.7 kg skipjack tuna) (Stevens, 1972; Strother, 2013a) in Appendix C revealed that in both specimens, the channel model estimate was very close to the *in vivo* measure, whereas the pore model estimate was approximately 1/2–1/3 of the measured value. These results exhibited that the discrepancy between the measured value and the theoretical estimate using the pore model was due to the inadequate theoretical expression of the pore-bound resistance (Eq. (A-18)). Moreover, the close agreement between the channel model estimate (Eq. (A-19)) and the measured value allowed us to rule out any massive bypassing flow outside the gills. The latter agreement also reinforced the validity of analyzing the gill lamellar system by the present channel model under steady-state water flow assumption.

The above explanations largely substantiate the acceptability of the assumptions made in the theoretical analyses. Some remarkable findings revealed in Results are summarized below.

In Fig. 5, the $\Delta\dot{Q}$ curve showed a peak against the water ventilation at Stage V ($F_w = F_{crit}$) (Supplement 2, Eqs. (S-4) and (S-5)). This finding indicates the upper-limit of the swimming activity of this fresh water fish, rainbow trout, because any further increase in F_w beyond F_{crit} decreases the O_2 supply to exercising muscles and induces an O_2 deficiency in them. Obviously, the high O_2 consumption rate by gill itself (κCF) is the main factor inducing such limit of activity.

The fast swimming oceanic fish species (*e.g.*, tuna) are known to have much higher physical activities than those in other fish groups including fresh-water fish (*e.g.*, rainbow trout), due to longer lamellae (by 1.5–2.0 times) and much ampler total gill surface areas (by nearly 10 times) than those in other groups (Wegner, 2011). Furthermore, the ram ventilation system in this fish group must diminish the κCF level, due to simpler ventilation mechanisms than those of the buccal/opercular pumping system in the other fish groups. This change may shift the peak of the $\Delta\dot{Q}$ curve in Fig. 5 to the right, associating the elevation of the critical (maximum) swimming velocity. These factors may afford higher physical activities to ram ventilators for swimming around all great oceans.

Returning to rainbow trout, its gill respiration within the limits seems to be very effectively performed for O_2 uptake and its delivery to the skeletal muscles. Fig. 4 shows that the relative efficiency (η_g^*) levels at Stages II ~ V were 0.95–1.00 (Table 2), indicating very high cost-performance for O_2 uptake due to the matching of F_w and F_b at every swimming Stage. The $w_{\min}$ points on the five $CF(w)$ curves in Fig. 3, being evenly distributed around the standard width ($w_s = 24$ μm), revealed that the excessive ratio (ε) in Eq. (12) never exceeded 10% of $CF(w_{\min})$ at any Stage. This implies that the standard width (w_s) is exquisitely selected *a priori* such that it can maintain $CF(w)$ largely at the optimum level at any swimming velocity. If these findings are confirmed in additional fishes, the gill lamellar system can be registered as a great example of optimally designed architectures in living organisms (Rosen, 1967).

Finally, the wall shear stress ($\bar{\tau}_s$) on the lamellar surface induced by the maximum water flow (F_{crit}) at Stage V was estimated to be approximately 25 dynes/cm^2 (Eq. (14)). This level of fluid shear stress is nearly equal to that exerted by blood flow on the vascular endothelial cell surface in the mammalian arterial tree (Kamiya and Togawa, 1980). It is now established that this blood flow-oriented shear stress is the key factor optimizing the entire arterial tree, as predicted in the minimum work or volume model (Murray, 1926; Kamiya and Togawa, 1972), by auto-regulating this stress constant through the adaptive remodeling of the vascular size (Kamiya and Ando, 1996). Recent molecular biological studies using cultured endothelial cells have reported various cytoplasmic responses induced by this stress (e.g., Yamamoto et al., 2006). It is not surprising that the fluid shear stress in the similar order may induce an adaptive remodeling responses in the fish gill lamellar system to keep the most effective structure for O_2 uptake and transport for achieving the highest physical activities in aquatic life.

Conflict of interest statement

This authors have no financial or personal conflicts of interest to disclose.

Acknowledgements

This work was partly supported by a Grand-in-Aid from the Japan Society for Atherosclerosis Research Foundation.

Appendix A

<Biomechanical derivation of the minimum work model. (Eqs. (1), (2), and (3) in the text)>

The pore model proposed by Hughes (1966) and our channel model represent the same morphological microstructure of the lamellar system (i.e., a pore consists of two channels connected opposite to each other).

According to the water ventilation mechanism, pressure and flow profiles in inter-lamellar channels may be different between the ram ventilation in fast swimming oceanic fish and the buccal/opercular pumping ventilation in other fish groups (Wegner, 2011). In the former case, the water flow pattern must be steady (Stevens and Lightfoot, 1986) whereas in the latter case, it must be more or less pulsatile even in the inter-lamellar spaces (Malte, 1992; Malte and Weber, 1985). It is, however, well known that in both cases, the inter-lamellar water flow is laminar because Reynolds number (Re) in it is very low ($Re < 10$) (Malte, 1989; Wegner, 2011). Thus, the cyclic changes in flow velocity at each point of a cross-section can be eliminated by calculating their integrated means over the respiratory cycle (Han et al., 2016). The obtained steady flow data may afford a clear flow velocity distribution in the inter-lamellar water channel which is a very feasible information to calculate an accurate estimate of the mechanical power expenditure through it as seen below.

As for the steady-state laminar flow of water in the gill system, the velocity distribution at any cross section of each inter-lamellar rectangular channel can be expressed by the quadratic function of the orthogonal coordinates (x, y) in Fig. 2:

$$u(x,y) = u_{\max}\left[1-\left(\frac{x}{w/2}\right)^2\right]\left[1-\left(\frac{y}{h}\right)^2\right], \quad u_{\max} = \frac{9f_w}{4wh}, \tag{A-1}$$

where $u_{\max}$ is the maximum flow velocity, and f_w is the water flow rate through a single channel. The ranges of the variables are; $[-w/2 \leqslant x \leqslant w/2, 0 \leqslant y \leqslant h]$.

The wall shear stress at the bottom of the rectangular water channel is expressed as,

$$\tau_b(x) = \left|\mu_w \frac{\partial u(x,y)}{\partial y}\right|_{y=h} = -\frac{9\mu_w f_w}{2wh^2}\left[1-4\frac{x^2}{w^2}\right],$$

in which μ_w is the viscosity of water. The average wall shear stress at the bottom of the water channel is then given as follows:

$$\bar{\tau}_b = \frac{1}{w}\int_{-w/2}^{w/2}\tau_b(x)dx = -3\frac{\mu_w f_w}{wh^2}. \tag{A-2}$$

Similarly, the wall shear stress at either sidewall of the water channel is expressed as follows:

$$\tau_s(y) = \left|\mu_w \frac{\partial u(x,y)}{\partial x}\right|_{x=\pm w/2} = -\frac{9\mu_w f_w}{w^2 h}\left[1-\frac{y^2}{h^2}\right]$$

and the average wall shear stress at a sidewall is then given by,

$$\bar{\tau}_s = \frac{1}{h}\int_0^h \tau_s(y)dy = -6\frac{\mu_w f_w}{w^2 h} \tag{A-3}$$

The Stokes equation concerning the equilibrium of fluid dynamic forces indicates that,

$$\Delta P_w hw + 2\bar{\tau}_s lh + \bar{\tau}_b wl = 0$$

where ΔP_w is the hydraulic pressure drop over the channel. By substituting $\bar{\tau}_b$ and $\bar{\tau}_s$ in Eqs. (A-2) and (A-3) into the above equation, we obtain the following:

$$\Delta P_w = 3\frac{l\mu_w f_w}{hw}\left(\frac{4}{w^2}+\frac{1}{h^2}\right) \tag{A-4}$$

We also assume that the internal anatomical structure of any single lamella including the vascular bed remains uniform regardless of the lamellar density. The blood pressure drop across the vascular bed in each lamella (ΔP_b) can then be written as follows:

$$\Delta P_b = \mu_b k_b f_b = r_b f_b \tag{A-5}$$

where f_b is the blood flow rate through a single lamella, and μ_b and k_b are the blood viscosity and structural factor due to the vasculature in each lamella, respectively. Accordingly, the term r_b $(= \mu_b k_b)$ indicates the vascular resistance in a single lamella.

The mechanical energy cost (CF) required for gill respiration is evaluated as the sum of the energy expenditure per time for water ventilation (F_w) and blood circulation (F_b) through the entire lamellar system over the gills, which can also be described as follows:

$$CF = \Delta P_w F_w + \Delta P_b F_b = R_w F_w^2 + R_b F_b^2 = \Delta P_w n f_w + \Delta P_b n f_b \tag{A-6}$$

where R_w and R_b indicate the total resistances to F_w and F_b through the gills, respectively, and n designates the total number of the inter-lamellar channel units in the entire gill system. The available morphometric parameters relevant to n include either the total surface area of the gill lamellae (A_g) or the total sum of the interlamellar widths of all water channels in the entire gills (L_g), because they are expressed as $[A_g = 2nhl]$ and $[L_g = nw]$, respectively. Assume that L_g is a constant parameter throughout the following theoretical analyses. This assumption implies that the whole size of the gills is maintained constant, whereas n and w are variables in mutual inverse proportion.

By substituting Eqs. (A-4) and (A-5) into Eq. (A-6), we obtain the following theoretical expression of $CF(w)$:

$$CF(w) = 3\frac{l}{h}\frac{\mu_w F_w^2}{L_g}\left(\frac{1}{h^2}+\frac{4}{w^2}\right)+\frac{r_b F_b^2}{L_g}w \tag{A-7}$$

The above equation is the basic formulation of $CF(w)$ as the analytical function of the inter-lamellar width (w) in this study, which corresponds to Eq. (1) in the text.

By assuming that parameters L_g, l, h, μ_w, F_w, r_b, and F_b in Eq. (A-7) are all constant, the minimizing condition of $CF(w)$ is derived by partially differentiating Eq. (A-7) with respect to w and setting the outcomes to zero:

$$\frac{\partial CF(w)}{\partial w} = -24\frac{l}{h}\frac{\mu_w F_w^2}{L_g}\frac{1}{w^3}+\frac{r_b F_b^2}{L_g} = 0$$

from which an explicit analytical solution of the minimizing width (w_{min}) is obtained as

$$w = \left[24\frac{\mu_w}{r_b}\frac{l}{h}\left(\frac{F_w}{F_b}\right)^2\right]^{1/3} = w_{\min} \tag{A-8}$$

which is referred as Eq. (2) in the text.

The resistance to water flow through a single channel (r_w), which is given from Eq. (A-4) as $[\Delta P_w/f_w]$, can be abridged by approximating it as

$$r_w = \frac{\Delta P_w}{f_w} = 3\frac{l}{h}\frac{\mu_w}{w}\left(\frac{1}{h^2}+\frac{4}{w^2}\right) \approx 12\frac{l}{h}\frac{\mu_w}{w^3} \tag{A-9}$$

because $1/h^2 << 1/w^2$. This approximate equation is cited as Eq. (3) in the text.

Appendix B

<Theoretical analyses of the cost performance and relative efficiency of gill respiration for O_2 uptake from water (Eqs. (4), (5) and (6) in the text).>

As described in the Introduction, the cost performance of O_2 uptake from water (η_g) is given by the ratio (total amount of O_2 uptake)/(biomechanical work required for gill respiration) and can be written as,

$$\eta_g = \frac{\dot{Q}}{CF} \tag{A-10}$$

in which CF is an abbreviation of $CF(w)$in Eq. (1) (or Eq. (A-6)) and $\overset{*}{Q}$ indicates the total amount of O_2 uptake. The numerator of Eq. (A-10) ($\dot{Q}$) is known to be predominantly perfusion limiting (Evans et al., 2005) and, according to Kiceniuk and Jones (1977), it can be expressed almost as a linear or a power function of the water ventilation rate (F_w) with the constant parameters k_0 and $\alpha(\ll 1)$:

$$\dot{Q} = k_0 F_w^{1-\alpha} \tag{A-11}$$

which corresponds to Eq. (5) in the text. The numerical values of k_0 and α are determined as ($k_0 = 2.83 \times 10^{-3}$ and $\alpha = 0.033$) from Eq. (S-2) in Supplement 1.

On the other hand, the denominator of Eq. (A-10) can be expressed from Eqs. (A-6) and (A-7) as

$$CF = R_m F_m^2 + R_b F_b^2 \tag{A-12}$$

From Eqs. (A-11) and (A-12), we obtain,

$$\eta_g = \frac{k_0 F_w^{1-\alpha}}{R_w F_w^2 + R_b F_b^2} \tag{A-13}$$

If we introduce a new variable [$\xi = F_w/F_b$] into Eq. (A-13), η_g is rewritten as,

$$\eta_g = \frac{k_0' \xi^{1-\alpha}}{R_w \xi^2 + R_b}, \text{where} \left[k_0' = \frac{k_0}{F_b^{1+\alpha}}\right], . \tag{A-14}$$

The maximizing condition of η_g can be then determined by partially differentiating Eq. (A-14) with respect to ξ and by setting the outcome to zero:

$$\frac{\partial \eta_g}{\partial \xi} = k_0' \xi^{-\alpha} \left[\frac{-(\alpha+1)R_w\xi^2 + (1-\alpha)R_b}{(R_w\xi^2 + R_b)^2}\right] = 0$$

Consequently, we find the following maximizing condition of η_g;

$$\xi_{\max} = \left(\frac{F_w}{F_b}\right)_{\max} = \left[\frac{(1-\alpha)}{(1+\alpha)}\frac{R_b}{R_w}\right]^{1/2} = \varphi \tag{A-15}$$

By substituting this maximizing factor ($\xi_{\max} = \varphi$) into Eq. (A-14), the highest efficiency ($\eta_{g,\max}$) is given as,

$$\eta_{g,\max} = \frac{k_0' \varphi^{1-\alpha}}{R_w \varphi^2 + R_b}$$

Eventually, the relative efficiency for O_2 uptake from water through the gill (η_g^*) is derived by normalizing η_g with $\eta_{g,\max}$, which can be rewritten as a unique function of parameter ξ ($= F_w/F_b$) as follows:

$$\eta_g^*(\xi) = \frac{\eta_g}{\eta_{g,\max}} = \left(\frac{\xi^{1-\alpha}}{R_w\xi^2 + R_b}\right) \Big/ \left(\frac{\varphi^{1-\alpha}}{R_w\varphi^2 + R_b}\right) \tag{A-16}$$

It is apparent from Eq. (A-16) that $\eta_g^*(\phi)$ is unity. Eq. (A-16) is given as Eq. (6) in the text and is utilized to depict the relative efficiency curve $\eta_g^*(\xi)$ in Fig. 4 by substituting the numerical values of α, R_w and R_b in Tables 1 and 2.

Appendix C

<Comparison of the estimates of total water flow resistance over the gills by the conventional pore model and by the present channel model with the actually measured data>

As described before, it is apparent that the pore model proposed by Hughes (1966) embodies the same geometrical structure of the interlamellar system as our channel model (a pore is composed of two channels connected upside down.)

The argument concerning the significant discrepancy between the theoretical estimate and actual measure of total water flow resistance (R_w) was proposed by Hughes (1966) using data in a tench with a body weight of approximately 140 g. In his original paper, the water pathway between the gills lamellar walls was regarded a straight rectangular tube (pore), and the steady-state pressure-flow relationship in pores was formulated by modifying Hagen–Poiseuille's law for a cylindrical tube. It was presented by the equation following:

$$q = \frac{P_1 - P_2}{\mu_w}\frac{5d^3 b}{24l}, \tag{A-17}$$

in which (q) and ($P_1 - P_2$) denote the water flow and pressure drop through a single rectangular pore with the size of the breadth (d), height (b) and length (l) while (μ_w) indicates water viscosity. From this equation, the water flow resistance through a single pore (r_w^p) is readily expressed as follows:

$$r_w^p = \frac{P_1 - P_2}{q} = \frac{24l\mu_w}{5d^3 b} \tag{A-18}$$

By substituting the data selected by Hughes (1966) from his own data table for a 140 g tench, namely, $l = 860$ μm, $d = 25$ μm, $b = 200$ μm, and $\mu_w = 1.3 \times 10^2$ dyn·s/cm^5 into Eq. (A-18), we obtain the following estimate of the resistance:

$$r_w^p = 1.72 \times 10^7 \text{dyn} \cdot \text{s/cm}^5$$

Furthermore, in the same table cited above, we found that the body-weight-specific total lamellar surface area of this fish (A_g^*) as [$A_g^* = 3.83\text{cm}^2/\text{g}$], which yields the total number of pores (N^p) as

$$N^p = A_g^* \times 140/(2lb) = 1.56 \times 10^5$$

The total water flow resistance through the whole pores (R_w^p) in parallel is calculated as follows:

$$R_w^p = \frac{r_w^p}{N^p} = 1.10 \times 10^2 \text{dyn} \cdot \text{s/cm}^5$$

On the other hand, the water flow resistance through a single interlamellar channel (r_w^c) in the present channel model has been approximated by Eq. (3) in the text (or Eq. (A-9) in the Appendix A) as follows:

$$r_w^c \approx \frac{12l\mu_w}{w^3 h} \tag{A-19}$$

By adopting the data in the tench as $l = 860$ μm, $w = d = 25$ μm, $h = b/2 = 100$ μm and by substituting them with $\mu_w = 1.3 \times 10^2 \text{dyn} \cdot \text{s/cm}^5$ into the above Eq. (A-19), we obtain,

$$r_w^c \approx 8.59 \times 10^7 \text{dyn} \cdot \text{s/cm}^5$$

From the A_g^* data in the 140 g tench, we have the total number of channels (N^c) as

$$N^c = 2N^p = 3.12 \times 10^5$$

These data eventually give the total water flow resistance through the entire channels (R_w^c) as

$$R_w^c = \frac{r_w^c}{N^c} = 2.75 \times 10^2 \mathrm{dyn \cdot s/cm^5}$$

The measured value of total water flow resistance through the entire gill (R_w^m) has been reported by Strother (2013a) for a 140 g tench as

$$R_w^m \approx 3 \times 10^7 \mathrm{Pas \cdot s/m^3} = 3 \times 10^2 \mathrm{dyn \cdot s/cm^5}$$

It is then evident that the water flow resistance through the present interlamellar channel model (R_w^c) is very close to the measured resistance through the entire gills (R_w^m), whereas the calculated resistance in the conventional pore model (R_w^p) is much less than the measured value (R_w^m) (nearly 1/3 of R_w^m).

Another feasible example to compare the actual measured total water flow resistance through the entire gill and the fluid-mechanical estimates of the resistance through it has been presented by Stevens and Lightfoot (1986) in skipjack tuna with a body weight of approximately 1.7 kg. These authors closely studied water flow through the pores and found that the flow pattern through them could be regarded steady, laminar, and creeping. Morphological data of the pores in the gill of this fish were listed as, $b = 2h = 127$ μm, $l = 1200$ μm and $N^p = N^c/2 = 7.18 \times 10^6$. By using these data and $\mu_w = 1.3 \times 10^2 \mathrm{dyn \cdot s/cm^2}$ again, we have r_w^p from Eq. (A-18) as

$$r_w^p = 6.36 \times 10^7 \mathrm{dyn \cdot s/cm^5}$$

whereas r_w^c is given from Eq. (A-19) as

$$r_w^c = 31.8 \times 10^7 \mathrm{dyn \cdot s/cm^5}$$

Consequently, the total water flow resistance values R_w^p and R_w^c are estimated as

$$R_w^p = \frac{r_w^p}{N^p} = 8.91 \,\mathrm{dyn \cdot s/cm^5}$$

and

$$R_w^c = \frac{r_w^c}{N^c} = 22.1 \,\mathrm{dyn \cdot s/cm^5}$$

Stevens (1972) reported that the relationship between the experimentally measured values of total ventilation (F_w) ($\mathrm{cm^3/s}$) and associated hydraulic pressure drop (ΔP_w) ($\mathrm{dyn/cm^2}$) over the entire gills in skipjack tuna of similar sizes could be expressed as

$$\Delta P_w = 22.7 F_w$$

From this, the total water flow resistance (R_w^m) is readily calculated as

$$R_w^m = \frac{\Delta P_w}{F_w} = 22.7 \,\mathrm{dyn \cdot s/cm^5}$$

This value well agrees with the above result ($R_w^c = 22.1 \,\mathrm{dyn \cdot s/cm^5}$) obtained using the present channel model, whereas the estimate ($R_w^p = 8.91 \,\mathrm{dyn \cdot s/cm^5}$) obtained using the pore model is much less than the above measured value (R_w^m).

Appendix D. Supplementary material

Supplementary data to this article can be found online at https://doi.org/10.1016/j.jbiomech.2019.03.033.

References

Ando, J., Ohtsuka, A., Korenaga, R., Kawamura, T., Kamiya, A., 1993. Wall shear stress rather than shear rate regulates cytoplasmic Ca^{++} responses to flow in vascular endothelial cells. Biochem. Biophys. Res. Commun. 190, 716–723.

Caro, C.G., Nerem, R.M., 1973. Transport of ^{14}C-4-cholesterol between serum and wall in the perfused dog common carotid artery. Circ. Res. 32, 187–205.

Davis, J.C., Cameron, J.N., 1971. Water flow and gas exchange at the gills of rainbow trout, Salmo gairdneri. J. Exp. Biol. 54, 1–18.

Eckert, D., Rundall, D., Augustine, G., 1988. Animal Physiology: Mechanisms and Adaptation. W. F. Freeman and Company, New York, pp. 435–519.

Evans, D.H., Piermarini, P.M., Choe, K.P., 2005. The multifunctional fish gill: dominant site of gas exchange, osmoregulation, acid-base regulation, and excretion of nitrogenous waste. Physiol. Rev. 85, 97–177.

Han, B., Hirahara, H., Yoshizaki, S., 2016. Streaming caused by oscillatory flow in peripheral airways of human lung. Open J. Fluid Dyn. 6, 242–261.

Hill, R.W., Wyse, G.A., Andersen, M., 2016. Animal Physiology. Sinauer Associates Inc, Massachusetts, pp. 585–719.

Hughes, G.M., 1960. A comparative study of gill ventilation in marine teleost. J. Exp. Biol. 37, 28–45.

Hughes, G.M., 1966. The dimensions of fish gills in relation to their function. J. Exp. Biol. 45, 177–195.

Hughes, G.M., 1972. Morphometrics of fish gills. Respir. Physiol. 14, 1–25.

Hughes, G.M., 1984. General anatomy of the gills. Fish Physiol. 10, 1–72.

Hughes, G.M., Morgan, M., 1973. The structure of fish gills in relation to their respiratory function. Biol. Rev. 48, 419–475.

Hughes, G.M., Shelton, G., 1958. The mechanism of gill ventilation in three freshwater teleost. J. Exp. Biol. 35, 807–823.

Kamiya, A., Ando, J., 1996. Response of vascular endothelial cells to fluid shear stress: mechanism. In: Hayashi, K., Kamiya, A., Ono, K. (Eds.), Biomechanics: Functional Adaptation and Remodeling. Springer-Verlag, Tokyo, pp. 29–56.

Kamiya, A., Togawa, T., 1972. Optimal branching structure of the vascular tree. Bull. Math. Biophys. 34, 431–438.

Kamiya, A., Togawa, T., 1980. Adaptive regulation of wall shear stress to flow change in the canine carotid artery. Am. J. Physiol. 239, H14–H21.

Kiceniuk, J.W., Jones, D.R., 1977. The oxygen transport system in trout (salmo gairdneri) during sustained exercise. J. Exp. Biol. 69, 247–260.

Malte, H., Weber, R.E., 1985. A mathematical model for gas exchange in the fish gill based on non-linear blood gas equilibrium curves. Respir. Physiol. 62, 359–374.

Malte, H., 1989. Pressure/flow relations in the interlamellar space of fish gills: theory and application in the rainbow trout. Respir. Physiol. 78, 229–241.

Malte, H., 1992. Effect of pulsatile flow on gas exchange in the fish gill: theory and experimental data. Respir. Physiol. 88, 51–62.

Murray, C.D., 1926. The physiological principle of minimum work: I. The vascular system and the cost of blood volume. Proc. Natl. Acad. Sci. USA 12, 207–214.

Olson, K.R., 2002. Gill circulation: regulation of perfusion distribution and metabolism of regulatory molecules. J. Exp. Zool. 293, 320–335.

Root, R.W., Irving, L., Black, E.C., 1939. The effect of hemolysis upon the combination of oxygen with the blood of some marine fishes. J. Cell Physiol. 13, 303–313.

Rosen, R., 1967. Optimality Principles in Biology. Butterworths, London, pp. 41–60.

Schmidt-Nielsen, K., 1990. Animal Physiology: Adaptation and Environment. Cambridge University Press, Cambridge, pp. 3–125.

Shibata, M., Ichioka, S., Ando, J., Togawa, T., Kamiya, A., 2005. Nonlinear regulation of capillary perfusion in relation to ambient pO_2 changes in skeletal muscle. Eur. J. Appl. Physiol. 94, 352–355.

Stevens, E.D., 1972. Some aspects of gas exchange in tuna. J. Exp. Biol. 56, 809–823.

Stevens, E.D., Lightfoot, E.N., 1986. Hydrodynamics of water flow in front of and through the gills of skipjack tuna. Comp. Biochem. Physiol. 83, 255–259.

Strother, J.A., 2013a. A computational model of flow between the microscale respiratory structures of fish gills. J Theor Biol 338, 23–40.

Strother, J.A., 2013b. Hydrodynamic resistance and flow patterns in the gills of a tilapine fish. J. Exp. Biol. 216, 2595–2606.

Wegner, N.C., 2011. Gill respiratory morphometrics. In: Farrell, A.P. (Ed.), Encyclopedia of Fish Physiology: from Genome to Environment. Academic Press, San Diego, CA, pp. 803–811.

Yamamoto, K., Sokabe, T., Matsumoto, T., Yoshimura, K., Shibata, M., Ohura, N., Fukuda, T., Sato, T., Sekine, K., Kato, S., Isshiki, M., Fujita, T., Kobayashi, M., Kawamura, K., Masuda, H., Kamiya, A., Ando, J., 2006. Impaired flow-dependent control of vascular tone and remodeling in P2X4-deficient mice. Nat. Med. 12, 133–137.